RESEARCH ARTICLE

National Science Open
2: 20220056, 2023
https://doi.org/10.1360/nso/20220056

Physics

Special Topic: Glasses—Materials and Physics

Compression induced crystal-to-glass transition in soft colloidal solids

Li Chen[1,2,3], Xiunan Yang[1,2], Mingcheng Yang[1,2], Chenhong Wang[1,2,4,*] & Ke Chen[1,2,5,*]

[1] *Beijing National Laboratory for Condensed Matter Physics and Key Laboratory of Soft Matter Physics, Institute of Physics, Chinese Academy of Sciences, Beijing 100190, China;*
[2] *University of Chinese Academy of Sciences, Beijing 100049, China;*
[3] *Cygnus Biosciences Co., Ltd., Beijing 100176, China;*
[4] *Beijing Tide Pharmaceutical Co., Ltd., Beijing 100176, China;*
[5] *Songshan Lake Materials Laboratory, Dongguan 523808, China*

*Corresponding authors (emails: wangchh1@tidepharm.com (Chenhong Wang); kechen@iphy.ac.cn (Ke Chen))

Received 9 October 2022; Revised 21 December 2022; Accepted 3 January 2023; Published online 27 April 2023

Abstract: Using colloidal particles with different thermosensitivities, we observe the transition from a crystalline solid to a disordered glass by tuning the size mismatch of the constituent particles in quasi-two-dimensional configurations. The transition is clearly identifiable by the correlation functions of the orientational order parameters and its susceptibilities. Different from typical order-to-disorder transitions such as melting, where the underlying mechanism involves the diffusion of defects, the disordered phase in the crystal-to-glass transition grows via a nucleation process. The disordered clusters grow in size as the particle mismatch increases, and eventually percolate the whole system, which signifies the qualitative change from an ordered crystal to a disordered glass.

Keywords: crystal-to-glass transtion, percolation, colloidal solids

INTRODUCTION

Phase transitions are often accompanied by change of structural orders, with profound impacts on the properties of materials. And changes of structural orders are often sought as indicators for phase transitions. In the cases of melting [1–6] or sublimation [7] of crystalline solids, the material undergoes obvious change of states, when the structures change from ordered crystalline lattice to disordered liquid or gas. In other cases, however, a crystal can be continuously transformed into a disordered solid or glass, by progressively introducing defects into the ordered structure by ion irradiation [8–10], doping [11, 12] or mechanical treatments [13–17] until no more long-range crystalline order left in the system. It is difficult to determine the point where a crystal qualitatively transforms into a glass, as the system remains in the solid state during these processes while the structure evolves continuously. Such methods of creating glasses from crystalline solids are in clear contrast to the conventional way of producing glasses by rapid quenching, when the system

continuously transitions from flowing liquids to solid glasses with little changes in the structures. The order-to-disorder transition in solids thus provides a unique opportunity to study the structure of glasses, with the underlying crystalline structure as a well-defined reference.

Colloids are an ideal model system to study structural orders during phase transitions. The melting of colloidal crystals in both 2D and 3D have been intensively studied *in-situ*, using temperature-sensitive Poly-*N*-isopropylacrylamide (PNIPAM) particles [1, 18–22]. Yunker *et al.* [12] show that a small fraction of dopants in a colloidal crystal is sufficient to give rise to strong dynamical heterogeneity, a hallmark of glassy materials. Similar emergence of glassy dynamics is also observed when bond strength disorder is introduced into a crystalline lattice [23]. In both these experiments, the structure of the system remains largely crystalline. Recent computer simulations by Zhang *et al.* [14] show that sharp transitions between polycrystals and disordered glasses can be achieved by progressively compressing a binary mixture of hard and soft particles. In the simulations, the soft particles can assume one of two diameters depending on the local stress, thus creating two distinctive length scales in the system. It is not clear if similar sharp transition can still be observed when the size of the particles changes continuously.

In this Research Article, we study the transition from a quasi-2D colloidal crystal to a colloidal glass by simultaneously increasing the size mismatch between the constituent particles and the packing fraction of the system, a process analogous to compression-induced crystal-to-glass transition. The order-to-disorder transition is identified by a peak in the fluctuations of hexagonal order parameter and the loss of the long-range correlations of the orientational order in the system. As the system remains in solid state, diffusion contributes little to the transition from ordered crystal to disordered glass, in contrast to the melting of crystals. The transition is facilitated by the generation and growth of disordered clusters with increasing particle size mismatch. The system qualitatively transforms into glass phase when the disordered clusters become connected and percolate the system.

EXPERIMENT

We employ PNIPAM hydrogel particles whose size increases with decreasing temperature. Two types of PNIPAM microspheres, denoted as type A and type B, are synthesized with different crosslinker densities, which result in different thermosensitivities of the particles [24]. A higher crosslinker density leads to a lower thermosensitivity. Figure 1 plots the temperature dependence of diameters of the two types of PNIPAM particles measured by dynamic light scattering. The steeper slope for particle B (red line) indicates higher temperature sensitivity than particle A (black line). The sizes of the two types of particles are close around 28.5°C. In the temperature range between 29°C and 24°C, the size ratio of the two types of PNIPAM particles varies from 0.94 to 1.33, covering the range needed for crystal-to-glass transition in two dimensions [25–28].

The samples consist of a binary mixture of type A and type B particles, with a number ratio $n_A/n_B = 3:2$. 0.5 μL colloidal suspension is placed between two glass coverslips, and spreads under the gravity and capillary forces, forming a monolayer. The samples are then hermetically sealed using optical glue (Norland 63). Before data acquisition, the samples are annealed at 28.5°C on a microscope stage for 3 h to obtain uniform crystalline structures. The temperature of the sample is controlled by a resistive objective heater (Bioptechs). The sample temperature is gradually lowered from 28.5°C to 24.0°C at steps of ~0.2°C, and

the structure of the sample evolves from ordered triangular lattice to disordered glass. The nominal packing fraction of the sample changes from 0.9 to 1.55 for the same range of temperature. Snapshots of the sample images are shown in the insets of Figure 1. At each temperature, images of the samples are digitally recorded using a CCD camera mounted on the microscope at 60 frames per second for 500 s. There are ~4000 particles in the field of view, whose positions are extracted using standard particle tracking technique [29]. During the experiments, the long-time mean-square-displacement (MSD) for all samples are less than 5% of the average particle separation, below the Lindemann melting criterion.

RESULTS AND DISCUSSION

Figure 2 shows the measured pair correlation function $g(r)$ and the Fourier transformation of the sample images at different temperatures. At 28.5°C, when the diameters of particles A and B are close, the sample structure exhibits clear features of a triangular crystal. The first three peaks of $g(r)$ correspond to the 1, $\sqrt{3}$ and 2 times, respectively, of the lattice constant. The bright discrete pattern with six-fold symmetry in the Fourier transformation also confirms that the sample is in crystalline state. As the temperature is lowered, the particles of the two species swell at different rates, which increases the size mismatch between particles and the overall stress in the sample. The $g(r)$ peaks broaden with temperature, and the second and third peaks eventually merge into a round peak at 27.9°C, which is a sign of order-to-disorder transition, as the distortion of the crystalline lattice becomes comparable to the particle separations [30–32]. When the temperature is further lowered, the $g(r)$ peaks at large distances vanish when long-range periodicity is completely lost, and the $g(r)$ curves become indistinguishable from those of typical colloidal glasses. The evolution of the system structure from ordered crystal to glass is also confirmed by the diffraction patterns, when the distinct point patterns blur into halo rings.

The crystalline order in the system is quantified by the bond orientational order parameter $\psi_6 = \frac{1}{N_{\text{tot}}} \sum_{j=1}^{N_{\text{tot}}} \sum_{k=1}^{nn} |e^{i6\theta_{jk}}|/nn$. Here, θ_{jk} is angle between the bond connecting nearest-neighboring particles j and k, and x-axis, nn is coordination number of reference particle j, and N_{tot} is the total number of particles [12, 33]. Figure 3A plots the evolution of ψ_6 when the sample temperature decreases from 28.5°C to 24°C. The averaged ψ_6 decreases from nearly 1, which corresponds to perfect crystalline order, to about 0.6, the

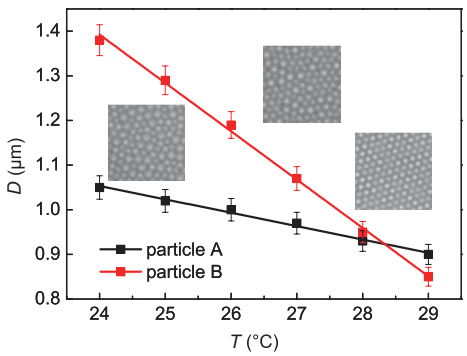

Figure 1 Temperature dependence of the diameters of PNIPAM microspheres with different thermosensitivities. The diameters are obtained by dynamic light scattering. Particle B (red squares) is more sensitive to temperature than particle A (black squares), the straightlines are linear fits to the measured data. Snapshots of sample structures at 28.5°C, 27.5°C, and 25.0°C are shown in the insets from right to left.

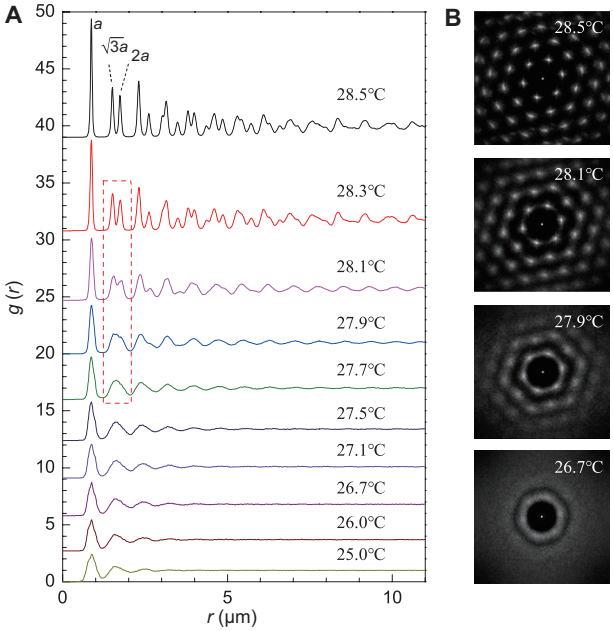

Figure 2 Evolution of structures during the crystal-to-glass transition. (A) The pair correlation function $g(r)$ at different temperatures. The merge of the second and third peaks (dotted rectangle) indicates the loss of crystalline order. (B) The diffraction patterns of the samples at four representative temperatures.

typical value for binary 2D glasses. Figure 3B plots the spatial correlation function of ψ_6, $g_6(r = |\mathbf{r}_i - \mathbf{r}_j|) = \langle \psi_{6i}^*(r_i)\psi_{6j}(r_j)\rangle$, where $\mathbf{r}_i$ and $\mathbf{r}_j$ are positions of particles i and j, and the angle bracket indicates ensemble average. At high temperatures when the particle mismatch is small, the envelope of g_6 decays following a power law, indicating long-range correlation of local orientational order. As the size mismatch increases, the g_6 starts to decay exponentially, as in the case of glasses. The change from a power law to exponential decay can be roughly determined between 27.9°C and 27.5°C.

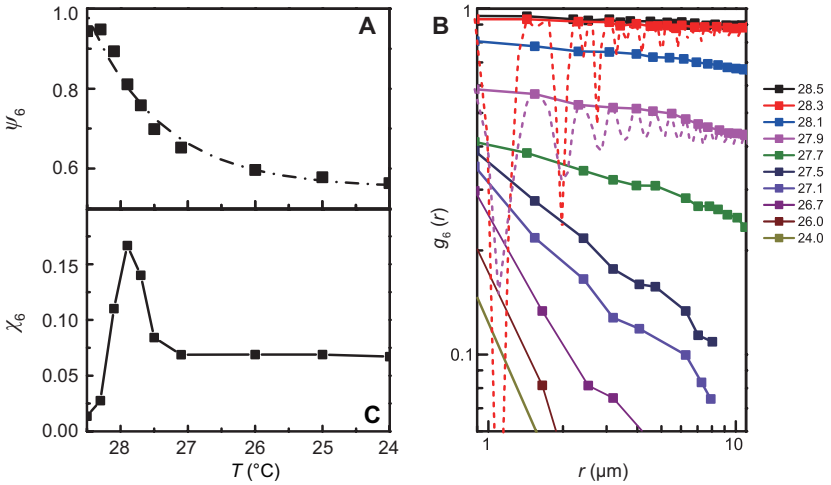

Figure 3 The evolution of the bond orientational order during the crystal-to-glass transition. (A) Bond orientational order ψ_6 as a function of sample temperature; (B) the envelope of the spatial correlation function g_6 at different temperatures; (C) the susceptibility of the bond orientational order, χ_6 as a function of temperature.

The temporal fluctuation of the bond orientational order is characterized by $\chi_6 = N_{\rm tot}(\langle(\bar{\psi_6})^2\rangle - \langle\bar{\psi_6}\rangle^2)$, where $\bar{\psi_6}$ is the averaged ψ_6 in a single frame, i.e., $\bar{\psi_6} = \sum_{j=1}^{N_{\rm tot}} |\psi_6|/N_{\rm tot}$, and bracket $\langle\rangle$ indicates time average. To avoid errors from finite size of the sample, we calculated a series of χ_6 within different size of sub-boxes, then extrapolated the χ_6 to infinite scale limit. The susceptibility χ_6 thus obtained is plotted in Figure 3C. A pronounced peak of χ_6 is observed at 27.9°C, signaling the order-to-disorder transition, and coincides with the structural crossover observed in $g(r)$ and $g_6(r)$.

The structural features shown in Figure 3 are similar to those observed in the melting of 2D colloidal crystals [21], but the microscopic mechanism in the solid order-to-disorder transition is fundamentally different. During the 2D melting, diffusion of the topological defects plays a critical role in creating an isotropic fluid from an anisotropic crystal [3, 4]. The defects are mostly dissociated disclination pairs created by the increased free volumes. During the crystal-to-glass transition, on the other hand, the defects are created by the compression of the lattices that reduces the overall free volume in the system, which then prohibits the diffusion of these defects. During the experiment, all the topological defects are "pinned" in place with no noticeable diffusions.

During the crystal-to-glass transitions, local crystalline order is progressively distorted when the disordered phase grows in size. The glass phase contains not only topological defects with 5 or 7 neighbors, but also distorted hexagonal units. We employ disordered clusters to quantify the structural evolution during the transition [14]. Specifically, a particle is considered ordered if it has three or more nearest neighbors with the product of the local bond order $|\psi^*_{6i}(r_i)\psi_{6k}(r_k)| \geqslant 0.65$; otherwise, it is considered disordered or a defect. This criterion is based on the observation that in 2D binary glasses, the typical $\langle\psi_6\rangle$ is ~0.6. Figures 4A–4D plot the spatial distribution of the ordered (blue) and disordered (red) particles at different temperatures. The disordered phase emerges from the crystalline background, and the two phases remain separated even after the disordered clusters percolate the whole system. Therefore, the crystal-to-glass transition occurs via one-step transition, instead of a two-step transition as the melting of 2D crystals.

As the temperature is lowered from 28.5°C, both the number and size of the disordered clusters increase, eventually percolating the whole system. Figure 5A plots the typical sizes of disordered clusters, the largest cluster size and the average cluster size, respectively, at different temperatures. The cluster size increases exponentially towards the percolation transition. Figure 5B plots the size distribution of disordered clusters at temperatures above $T = 27.7$°C. The fraction of large clusters increases as the temperature decreases, and the distributions can be well fitted to a power law truncated by an exponential function. We compare the size distribution of disordered clusters to that of randomly generated clusters. Specifically, after the fraction of disordered particles is determined from experiments, the same fraction of particles in a certain frame is randomly tagged as disordered particles. The particles are then grouped into disordered clusters based on their spatial proximity so that neighboring disordered particles belong to the same disordered cluster. The size distributions of the disordered clusters are qualitatively different from those of randomly generated clusters of the same configurations, as shown in the inset of Figure 5B, with much higher probability at large n, which suggests that as the system is progressively compressed, new disordered particles emerge not randomly, but preferentially next to existing large clusters. The disordered clusters thus act as "nuclei" of the disordered phase until they percolate the whole system, when the system qualitatively transitions from an ordered crystal to a disordered glass. This preferential attachment to existing disordered clusters is probably due to the stress localization near the boundary, which makes it easier to generate a disordered particle near

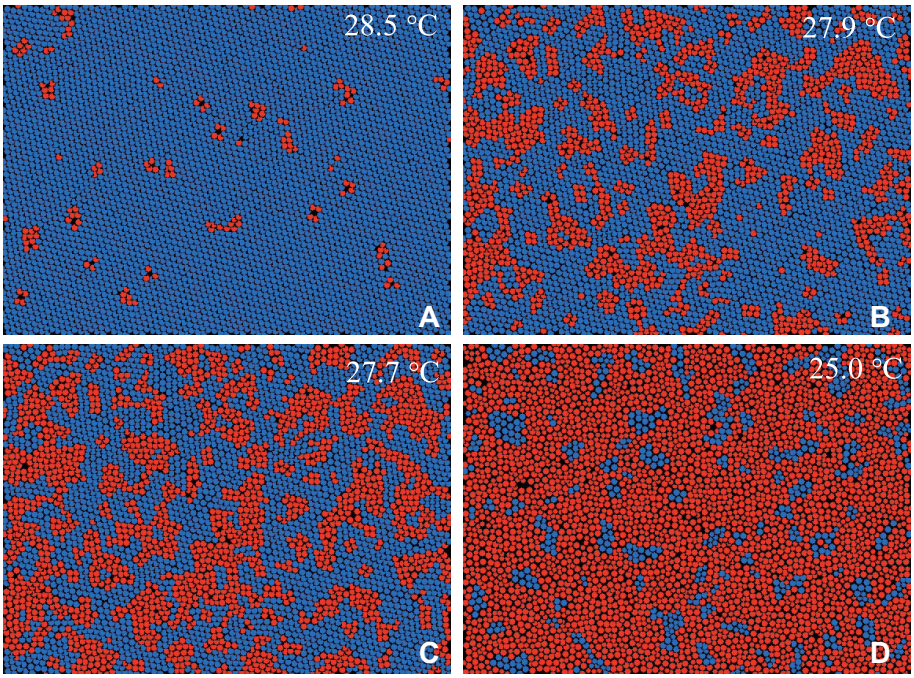

Figure 4 The distribution of disordered clusters at different temperatures. Particles in disordered clusters are shown in red, while regions with high crystalline order are shown in blue.

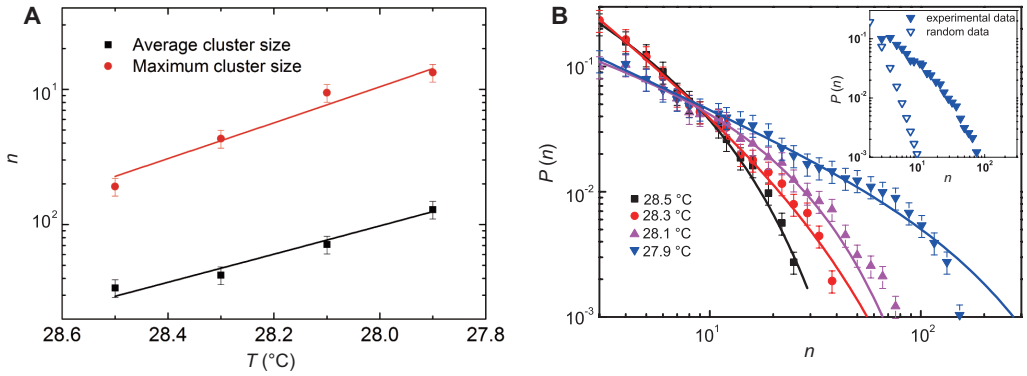

Figure 5 Sizes of disordered clusters. (A) Typical cluster sizes, including average sizes (black squares) and maximum sizes (red solid circles), as a function of sample temperature; (B) size distribution of disordered clusters at different temperatures. The distributions are fitted to a power law with exponential truncation (solid lines). (Inset) Comparison between the cluster size distributions obtained in experiments (solid triangles) and randomly generated clusters (empty triangles).

the boundary than inside the crystalline domain. The rapid growth of cluster sizes is driven by the increasing length of boundary between the ordered and disordered phases, and the inter-connection of existing clusters by a few disordered clusters approaching the percolation transition. Figure 6 plots the measured percolation probability of the disordered clusters. For each frame, the percolation status for the disordered clusters is determined. The percolation probability is defined as the fraction of time the disordered clusters are found to percolate the system during the experiment time window, with $P = t_p/t_{\text{tot}}$ where t_p is the number of frames that "percolated disordered cluster" occurs at a certain temperature, and t_{tot} is total frame number of measurement, which is ~30,000 in our experiments. The percolation probability jumps sharply from near

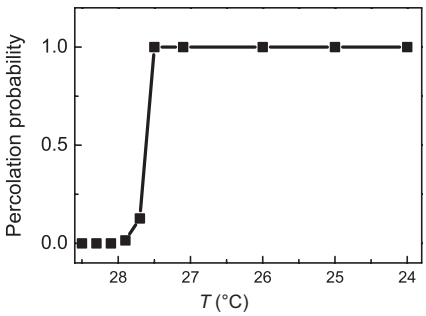

Figure 6 Percolation probability of the disordered clusters as a function of temperature.

zero to unity between 27.9°C and 27.5°C, in the same range where the χ_6 indicates a qualitative transition from crystalline phase to glass phase. The range of temperature for the percolation transition is practically the same when the threshold of the criterion for disordered particles changes from 0.6 to 0.7.

CONCLUSIONS

In summary, we employ PNIPAM colloidal particles with different thermosensitivities to study compression-induced crystal-to-glass transition in solid in a quasi-2D system. Compression creates disordered clusters in the crystalline background, which grow in size and numbers until eventually percolate the system. The percolation of the disordered clusters coincides with the qualitative transition from crystal to glass identified by the structural signatures and corresponding susceptibility. This one-step transition is qualitatively different from the two-step melting of crystals at 2D. It is also in contrast to the conventional glass transition, where the boundary between the liquid and solid phases is vague. In practice, qualitatively altering the structures of a solid by compression usually requires extremely high pressure, and some recent studies have shown evidence of order-to-disorder transition in solid materials [34]. In these experiments, the evolution of the structures on atomic level is difficult to assess. The thermo-sensitive colloids thus provide a convenient model to study the microscopic details of these phenomena. The change of dynamical and thermodynamical properties such as phonon modes during the crystal-glass transition are worthy of further studies in the future.

Funding

This work was supported by the National Natural Science Foundation of China (11874395 and 12174434) and the Strategic Priority Research Program of Chinese Academy of Sciences (XDB33000000).

Author contributions

K.C. and C.W. conceived the concept. C.W. and L.C. carried out the experiments. All the authors participated in the analysis of the experimental data. K.C. and L.C. prepared the manuscript.

Conflict of interest

The authors declare no conflict of interest.

References

1 Alsayed AM, Islam MF, Zhang J, *et al*. Premelting at defects within bulk colloidal crystals. *Science* 2005; **309**: 1207–1210.

2 Wang Z, Wang F, Peng Y, *et al*. Imaging the homogeneous nucleation during the melting of superheated colloidal crystals. *Science* 2012; **338**: 87–90.

3 Halperin BI, Nelson DR. Theory of two-dimensional melting. *Phys Rev Lett* 1978; **41**: 121–124.

4 Nelson DR, Halperin BI. Dislocation-mediated melting in two dimensions. *Phys Rev B* 1979; **19**: 2457–2484.

5 Strandburg KJ. Two-dimensional melting. *Rev Mod Phys* 1988; **60**: 161–207.

6 Chui ST. Grain-boundary theory of melting in two dimensions. *Phys Rev B* 1983; **28**: 178–194.

7 Savage JR, Blair DW, Levine AJ, *et al*. Imaging the sublimation dynamics of colloidal crystallites. *Science* 2006; **314**: 795–798.

8 Ossi PM. Crystal-glass phase transition in ion irradiated binary systems. *Phys Stat Sol (a)* 1990; **119**: 463–470.

9 Lu C, Jin K, Béland LK, *et al*. Direct observation of defect range and evolution in ion-irradiated single crystalline Ni and Ni binary alloys. *Sci Rep* 2016; **6**: 19994.

10 Jiang C, Zheng MJ, Morgan D, *et al*. Amorphization driven by defect-induced mechanical instability. *Phys Rev Lett* 2013; **111**: 155501.

11 Nelson DR, Rubinstein M, Spaepen F. Order in two-dimensional binary random arrays. *Philos Mag A* 1982; **46**: 105–126.

12 Yunker P, Zhang Z, Yodh AG. Observation of the disorder-induced crystal-to-glass transition. *Phys Rev Lett* 2010; **104**: 015701.

13 Wang YC, Zhang W, Wang LY, *et al*. *In situ* TEM study of deformation-induced crystalline-to-amorphous transition in silicon. *NPG Asia Mater* 2016; **8**: e291.

14 Zhang H, Han Y. Compression-induced polycrystal-glass transition in binary crystals. *Phys Rev X* 2018; **8**: 041023.

15 Wang Y, Zhu J, Yang W, *et al*. Reversible switching between pressure-induced amorphization and thermal-driven re-crystallization in VO2(B) nanosheets. *Nat Commun* 2016; **7**: 12214.

16 Bustingorry S, Jagla EA. Pressure-induced amorphization, crystal-crystal transformations, and the memory glass effect in interacting particles in two dimensions. *Phys Rev B* 2005; **71**: 224119.

17 Ourmazd A, Bean JC. Observation of order-disorder transitions in strained-semiconductor systems. *Phys Rev Lett* 1985; **55**: 765–768.

18 Alsayed AM, Han Y, Yodh AG. Melting and geometric frustration in temperature-sensitive colloids. In *Microgel Suspensions*. John Wiley & Sons, Ltd., 2011; **10**: 229–281.

19 Peng Y, Wang ZR, Alsayed AM, *et al*. Melting of multilayer colloidal crystals confined between two walls. *Phys Rev E* 2011; **83**: 011404.

20 Peng Y, Wang Z, Alsayed AM, *et al*. Melting of colloidal crystal films. *Phys Rev Lett* 2010; **104**: 205703.

21 Han Y, Ha NY, Alsayed AM, *et al*. Melting of two-dimensional tunable-diameter colloidal crystals. *Phys Rev E* 2008; **77**: 041406.

22 Zahn K, Lenke R, Maret G. Two-stage melting of paramagnetic colloidal crystals in two dimensions. *Phys Rev Lett* 1999; **82**: 2721–2724.

23 Gratale MD, Yunker PJ, Chen K, *et al*. Phonons in two-dimensional colloidal crystals with bond-strength disorder. *Phys Rev E* 2013; **87**: 052301.

24 Yunker PJ, Chen K, Gratale MD, *et al*. Physics in ordered and disordered colloidal matter composed of poly(*N*-isopropylacrylamide) microgel particles. *Rep Prog Phys* 2014; **77**: 056601.

25 Li M. Defect-induced topological order-to-disorder transitions in two-dimensional binary substitutional solid solutions: A molecular dynamics study. *Phys Rev B* 2000; **62**: 13979–13995.

26 Hamanaka T, Onuki A. Transitions among crystal, glass, and liquid in a binary mixture with changing particle-size ratio

and temperature. *Phys Rev E* 2006; **74**: 011506.

27 Hamanaka T, Onuki A. Heterogeneous dynamics in polycrystal and glass in a binary mixture with changing size dispersity and composition. *Phys Rev E* 2007; **75**: 041503.

28 Bocquet L, Hansen JP, Biben T, *et al*. Amorphization of a substitutional binary alloy: a computer "experiment". *J Phys-Condens Matter* 1992; **4**: 2375–2387.

29 Crocker JC, Grier DG. Methods of digital video microscopy for colloidal studies. *J Colloid Interface Sci* 1996; **179**: 298–310.

30 Kawasaki T, Araki T, Tanaka H. Correlation between dynamic heterogeneity and medium-range order in two-dimensional glass-forming liquids. *Phys Rev Lett* 2007; **99**: 215701.

31 Tanaka H. Roles of bond orientational ordering in glass transition and crystallization. *J Phys-Condens Matter* 2011; **23**: 284115.

32 Alsayed AM, Yodh AG. Two-dimensional freezing criteria for crystallizing colloidal monolayers. *J Chem Phys* 2010; **132**: 154501.

33 Yonezawa F, Ninomiya T. *Topological Disorder in Condensed Matter*. Berlin, Heidelberg: Springer, 1983

34 Deng Z, Kang C, Croft M, *et al*. A pressure-induced inverse order-disorder transition in double perovskites. *Angew Chem Int Ed* 2020; **59**: 8240–8246.